Fuel Processing Technology 286 (2026) 108435

Contents lists available at ScienceDirect

Fuel Processing Technology

journal homepage: www.elsevier.com/locate/fuproc

Research article

Large eddy simulation of auto-igniting methanol/n-dodecane blend spray flames

Bishal Shrestha [a,*], Fatimoh Balogun [b], Kevin Wan [c], Junghwa Yi [c], Huaying Wang-Alho [b], Shervin Karimkashi [a], Katriina Sirvio [b], Julien Manin [c], Maciej Mikulski [b], Jari Hyvönen [d], Ossi Kaario [a]

[a] Energy Conversion and Systems, Department of Energy and Mechanical Engineering, Aalto University, Otakaari 4, Espoo, 02150, Finland
[b] Efficient Powertrain Solutions (EPS), School of Technology and Innovation, University of Vaasa, Wolffintie 34, Vaasa, 65200, Finland
[c] Combustion Research Facility, Sandia National Laboratories, 7011 East Avenue, Livermore, CA, 94550, The United States of America
[d] Research and Technology Development, Wärtsilä Oy, Teollisuuskatu 1, Vaasa, 65170, Finland

ARTICLE INFO

Keywords:
Methanol/n-dodecane blends
ECN spray D
Experimental validation
Combustion
Adaptive mesh refinement

ABSTRACT

The study investigates the auto-ignition characteristics of methanol/n-dodecane fuel blends at varying blend ratios and ambient temperatures using large eddy simulation (LES) in OpenFOAM with the Engine Combustion Network (ECN) Spray-D injector. The primary objective is to determine the maximum methanol fraction in the blend that enables stable combustion with an engine-relevant ignition delay time (IDT) below 1 ms at ambient temperatures of 900, 950, 1000, and 1100 K. The numerical framework validation is performed against existing ECN n-dodecane data, new ECN experiments for pure methanol, and new methanol–octanol–diesel blend experiments from the Combustion Research Unit (CRU). Four cases satisfy the IDT criterion:

(I) 10% methanol, 90% n-dodecane at 900 K, (II) 20%–80% at 950 K, (III) 30%–70% at 1000 K, and (IV) 70%–30% at 1100 K. Increasing the methanol content suppresses ignition due to methanol's high heat of vaporisation and net consumption of OH radical at low temperatures. Ignition occurs under rich conditions for cases I and II, near stoichiometric conditions for case III, and under lean conditions for the methanol-dominant case IV. Case IV exhibits elevated centre-line temperature, increased NO emissions, and reduced C_2H_2 formation. Despite these differences, all cases display a similar heat release rate at quasi steady-state.

1. Introduction

Several combustion strategies, including dual–fuel (DF) [1,2] and blended-fuels [3,4] have been proposed to improve efficiency and reduce emissions in compression ignition (CI) engines. Methanol (CH_3OH) has attracted attention due to its lower emissions [5,6], sustainable production pathways [7–9], and ease of storage relative to hydrogen. However, the low cetane number and high heat of vaporisation of methanol hinder its ignition stability, resulting in a higher hydrocarbon (HC) emissions [5,10]. The poor ignitability of methanol can be mitigated using an ignition improver, such as diesel, to enhance the ignition quality [11–13]. This paper investigates the combustion characteristics of methanol and n-dodecane (surrogate to diesel) blends under engine-like conditions through high-fidelity large eddy simulation (LES) technique in OpenFOAM.

Experiments investigating methanol/diesel blends have shown that increasing the methanol fraction enhances the heat release rate (HRR) and in-cylinder pressure at high loads [13,14]. However, at low loads, a higher methanol fraction prolonged ignition and reduced cylinder pressure. Similarly, Garcia et al. [15] observed unstable combustion for pure methanol at low engine loads, noting the requirement of additional heat to sustain a stable combustion. However, at medium to high loads, the combustion sustained without any supplementary heat. These studies reveal a strong temperature-sensitive nature of methanol combustion. Furthermore, experimental studies [16,17] reported increasing NOx and reduced unburnt hydrocarbons with higher methanol percentage at high engine load. Another challenge associated with methanol/diesel blends is their immiscibility; experimental studies commonly employ emulsifiers such as 1-dodecanol [18] to ensure blend stability.

Regarding the ignition characteristics of pure methanol, a fundamental study [10] revealed that the large heat of vaporisation of methanol reduces the temperature in the spray core, leading to an

* Corresponding author.
E-mail address: bishal.shrestha@aalto.fi (B. Shrestha).

https://doi.org/10.1016/j.fuproc.2026.108435
Received 12 February 2026; Received in revised form 13 March 2026; Accepted 17 March 2026
Available online 4 April 2026

improper decomposition of H_2O_2, causing local combustion instability and prolonging the ignition delay time (IDT). Numerical analysis [19] attributed the ignition-inhibiting behaviour to methanol's high net consumption of OH radicals during low-temperature combustion. Additionally, studies [20,21] have reported that methanol's high heat of vaporisation and low boiling point yield denser sprays with shorter penetration length.

Kaario et al. [22] performed large eddy simulation (LES) of pure methanol and n-dodecane sprays under high-pressure, high-temperature conditions and compared their ignition behaviour. In numerical studies, diesel is commonly represented using a surrogate such as n-dodecane or n-heptane [23,24]. Kaario et al. reported two-stage ignition behaviour for methanol under lean and high-pressure conditions. Additionally, the study illustrated that the ignition of n-dodecane occurs faster and at rich regions, whereas methanol tends to ignite slower and at leaner regions.

Capturing such interactions in numerical simulations reliably and accurately requires validation of the spray model against well-defined experimental configurations. Kaario et al. [22] validated the spray model with experiments for pure n-dodecane from the Engine Combustion Network (ECN). ECN [25] provides an open-access data repository that contains baseline target conditions and standardised post-processing guidelines for spray studies. Similar to the ECN, the Combustion Research Unit (CRU) [26,27] replicates diesel engine-like conditions and also offers valuable data for reacting spray studies, such as pressure-rise and ignition delay time. The open-source CFD platform OpenFOAM [28] provides a computational framework for conducting such simulations. Consequently, the datasets from ECN and the OpenFOAM platform have been widely adopted for the spray combustion studies [29–31].

Sun et al. [32] performed a methanol spray simulation in a n-heptane/air mixture and showed temperature-sensitive nature of methanol. The study also validated the spray model for pure methanol and n-heptane sprays with ECN datasets, including vapour penetration, ignition delay time (IDT), and flame lift–off length (FLOL). The vapour penetration and IDT exhibited good correspondence, but discrepancies in FLOL were observed. A similar LES study by Karimkashi et al. [33] investigated methanol/air and methane/air combustion with n-dodecane pilot spray, and observed a longer IDT for the n-dodecane pilot in a methanol/air environment compared to the n-dodecane combustion in air (validated with ECN Spray A reference case). The study identified a narrow ignition window for methanol/diesel operation, due to strong OH-radical sensitivity.

Existing literature provides a combustion analysis of methanol/n-dodecane blends in a compression ignition (CI) engine environment, reporting ignition instability and prolonged IDT at high methanol fractions and low ambient temperatures. However, the methanol percentage and corresponding ambient temperatures at which the ignition stability begins to occur remain unexplored. The current study aims to evaluate the maximum methanol fraction in the methanol/n-dodecane blend so that the mixture ignites reliably and within the engine-relevant ignition times (IDT < 1 ms). The present study will perform a high-fidelity LES analysis of methanol/n-dodecane blend sprays under the validated ECN Spray D conditions. The specific objectives of the study are:

1. to validate the spray model for pure methanol and n-dodecane fuels against new and existing data from the ECN, respectively;
2. to compare the IDT obtained from previously unpublished CRU experiments with the methanol/n-dodecane LES results;
3. to quantify the maximum methanol fraction in the blend for proper combustion and to satisfy the ignition criteria (IDT < 1 ms) across various ambient temperatures (900, 950, 1000, and 1100 K);
4. to investigate the combustion characteristics of the blends at varying mixture ratios and ambient temperatures.

2. Methodology

2.1. 0D homogeneous reactor analysis

Prior to the large eddy simulation (LES) analysis, the present study employs Cantera [34] to evaluate the combustion characteristics of methanol/n-dodecane blends following established modelling assumptions, called the mixing-line concept in 0D homogeneous reactors [22,33,35,36]. In the mixing-line concept, the temperature resulting from fuel/air mixing is expressed as a function of the mixture fraction (Z) [37]. The concept identifies the most reactive mixture fraction (Z_{MR}) – corresponding to the lowest ignition delay time (IDT_{MR}) – which describes how the auto-ignition chemistry may prefer a particular mixture fraction, different from the stoichiometric mixture fraction. The IDT is defined as the time of maximum pressure gradient.

The setup contains a cold stream of methanol/n-dodecane blends at the temperature (T_{fuel}) of 363 K, referred to as the fuel stream, and a hot ambient air stream with 21% O_2 and $\rho = 22.8$ kg m^{-3}, mentioned as the ambient. The two streams mix adiabatically in a homogeneous reactor (`IdealGasReactor` in cantera). The blending ratio of the fuel stream mixture is varied from 0% methanol/100% n–dodecane to 100% methanol/0% n-dodecane in 5% increments of methanol fraction. The mixture fraction (Z) is varied from a lean mixture (Z = 0.02) to a rich mixture (Z = 0.2). The stoichiometric mixture fraction (Z_{st}) ranges from 0.061 for pure n-dodecane to 0.13 for pure methanol. Additionally, different ambient temperatures (900, 950, 1000, 1100 K) are tested in this setup. This analysis assists in the selection of cases for 3D LES simulations and is elaborated in Section 4.1.

2.2. 3D LES simulation

2.2.1. Numerical methods

The LES formulation of the governing equations, i.e., Favre filtered continuity, momentum, species, and energy equations, is given below:

$$\frac{\partial \overline{\rho}}{\partial t} + \frac{\partial \overline{\rho}\tilde{u}_i}{\partial x_i} = \overline{S_p}, \tag{1}$$

$$\frac{\partial \overline{\rho}\tilde{u}_i}{\partial t} + \frac{\partial (\overline{\rho}\tilde{u}_i\tilde{u}_j)}{\partial x_j} = \frac{\partial}{\partial x_j}(-\overline{p}\delta_{ij} + \overline{\rho}\tilde{u}_i\tilde{u}_j - \overline{\rho}\widetilde{u_i u_j} + \overline{\tau_{ij}}) + \overline{S_{u_i}}, \tag{2}$$

$$\frac{\partial \overline{\rho}\widetilde{Y_k}}{\partial t} + \frac{\partial (\overline{\rho}\tilde{u}_i\widetilde{Y_k})}{\partial x_i} = \frac{\partial}{\partial x_i}(\overline{\rho}\tilde{u}_i\widetilde{Y_k} - \overline{\rho}\widetilde{u_i Y_k} + \overline{\rho}\tilde{D}\frac{\partial \widetilde{Y_k}}{\partial x_i}) + \overline{S_{Y_k}} + \overline{\omega_k}, \tag{3}$$

$$\frac{\partial \overline{\rho}\tilde{h}_t}{\partial t} + \frac{\partial (\overline{\rho}\tilde{u}_j\tilde{h}_t)}{\partial x_j} = \frac{\partial \overline{p}}{\partial t} + \frac{\partial}{\partial x_j}(\overline{\rho}\tilde{u}_j\tilde{h}_s - \overline{\rho}\widetilde{u_j h_s} + \frac{\overline{\lambda}}{\overline{c_p}}\frac{\partial \tilde{h}_s}{\partial x_j}) + \overline{S_h} + \overline{\omega_h} \tag{4}$$

where $\overline{\rho}$, $\tilde{u}_i$, $\widetilde{Y_k}$, $\tilde{h}_s$, $\tilde{h}_t$ and $\overline{\tau_{ij}}$, denote filtered density, velocity, pressure, mass fraction of the species k, sensible enthalpy, total enthalpy and viscous stress tensor, respectively. The tilde (~) represents a Favre averaging, while the overbar (–) symbolises an LES spatial filtering. $\overline{\omega_k}$ and $\overline{\omega_h}$ are the production rates of each species k and heat release rate (HRR) respectively. In addition, $\overline{\omega_h} = \sum_k \Delta h^0_{f,k}\overline{\omega_k}$, where $\Delta h^0_{f,k}$ is the enthalpy of formation, and diffusion coefficient $D = \lambda/(\rho c_p)$. $\overline{S_p}$, $\overline{S_{u_i}}$, $\overline{S_{Y_k}}$, $\overline{S_h}$ are the source terms, which allow coupling between the liquid and gaseous phases in mass, momentum, species, and energy equations, respectively. In Eq. (4), $\overline{c_p}$ and $\overline{\lambda}$ represent the specific heat capacity and thermal conductivity of the mixture, respectively. Finally, the ideal gas law and the thermal equation of state close the system of equations.

The present study employs the finite-volume method within the OpenFOAM-12 [28] framework to solve Eqs. (1) to (4). The `PIMPLE` algorithm [38,39] solves the pressure and velocity. The study adopts the implicit–LES (ILES) approach, where the subgrid-scale (SGS) can be modelled by selecting a dissipative discretisation scheme. In addition, the cell size acts as the filter width, and the smallest resolved turbulent eddies are twice the cell size.

A second-order accurate Gamma scheme [40] with $k = 0.33$ is used for the convective terms. For time integration, the study applies a second-order scheme, while a second-order central discretisation scheme is used for the diffusion terms. The setup is consistent with the previous works published by our research group [29–31,36,41,42].

Table 1
Operating parameters for the three-dimensional large eddy simulation (LES) and experimental cases considered in this study.

LES cases			
	ECN Spray D [48]	Fuel blend	Unit
Fuel	CH_3OH	CH_3OH : $C_{12}H_{26}$	
Blending ratios	100%	Provided in Table 2	
Temperature	1000–1200	900–1100	[K]
Density	22.8	22.8	[kg m^{-3}]
Injection pressure	150	150	[MPa]
O_2	0%–15%	21%	[% mol]
Experimental cases			
	ECN Spray D [48]	Combustion Research Unit (CRU)	
Fuel	CH_3OH	CH_3OH : diesel : $C_8H_{17}OH$	
Injector type	Bosch 3–22	Bosch DLLA 158 P1281	
Blending ratios	100%	**Exp-I :** 9% : 77% : 14%	
		Exp-II : 17% : 69% : 14%	[% w]
		Exp-III : 29% : 48% : 23%	
ambient Pressure	6–7*	7	[MPa]
Temperature	1000–1200	923/973/973**	[K]
O_2	0%–15%	21%	[% mol]

* Target density of 22.8 kg m^{-3} is aimed, therefore the ambient pressure ranges from 6–7 MPa.
** The temperatures correspond to Exp-I, Exp-II, and Exp-III, respectively.

Table 2
Summary of the cases selected for LES simulations and their corresponding first-stage ignition delay from LES ($\tau_{1,\mathrm{LES}}$), second-stage ignition delay from LES ($\tau_{2,\mathrm{LES}}$), most reactive ignition delay time from 0D simulations ($\tau_{2,0\mathrm{D}}$), and the flame lift-off length (FLOL).

Case	Fuel blend [%w]		T_{amb}	$\tau_{1,LES}$	$\tau_{2,LES}$	$\tau_{2,0d}$	FLOL	$\frac{\tau_{2,LES}}{\tau_{2,0d}}$	$\frac{\tau_{2,LES}}{\tau_{1,LES}}$
	CH_3OH	$C_{12}H_{26}$	[K]	[ms]	[ms]	[ms]	[mm]		
I	10%	90%	900	0.127	0.58	0.162	29.06	3.58	4.56
II	20%	80%	950	0.134	0.65	0.11	30.37	5.91	4.85
III	30%	70%	1000	0.119	0.8	0.086	30.29	9.3	6.72
IV	70%	30%	1100	0.584	0.99	0.15	26.04	6.65	1.7

* $\tau_{1,LES}$ is the time when 20% of CH_2O_{max} is reached, while $\tau_{2,LES}$ is the time at which $P_{rise} = 0.1\ bar$.
** $FLOL$ is the first location where 2% of the radially and time-averaged maximum OH is obtained. Further details are provided in the supplementary materials (Section 7).

2.2.2. Computational setup

The present study adopts the ECN Spray A and D as baseline cases. The study validates the spray model for pure n-dodecane against existing ECN Spray A and D measurements [43–46] and for methanol with new Spray D experiments [47]. The validation results are presented in Sections 3.1, and 3.2, respectively, while the operating conditions and the injection parameters are provided in Table 1 and the ECN website: https://ecn.sandia.gov/.

After validation of the spray model for pure methanol and n-dodecane, the study investigates methanol/n-dodecane blends under the ECN Spray D conditions. A mixture of n-dodecane and methanol replaces the pure fuels in the Spray D simulations. The mass fraction of the blends is adjusted in the injected parcels. The details of modelling parameters are described in Section 2.2.4.

The present study simplifies the complex combustion chamber to a cylinder with a length and diameter of 200 mm and 100 mm. Fig. 1(a) illustrates a section of the domain, highlighting the mesh, static refinement zones (R2 and R3), refinement levels, and their corresponding dimensions. The base mesh starts from 4 mm and the two initial refinement zones, R2 and R3, result in the mesh resolutions of 125 μm and 250 μm, respectively. The setup, excluding the R1 refinement zone (depicted in Fig. 1(a)), produces approximately 9.5 million cells.

2.2.3. Dynamic mesh and load balance

In addition to the static refinement zones (R2 and R3), the study adopts adaptive mesh refinement (AMR) (R1 in Fig. 1(b)) functionality along with dynamic load balancing employing `PARMETIS` [49] in OpenFOAM. The mesh is refined/unrefined based on the mass fraction of fuel and temperature. This approach additionally refines the mesh (described in Section 2.2.2), achieving a mesh resolution of 62.5 μm in the spray area, and depicted in Fig. 1(b). Studies [31,50] have reported that the resolution of 62.5 μm resolves the important turbulent eddies in sprays.

The R1 refinement occurs up to 50 mm downstream of the nozzle, covering key spray processes including liquid droplet evaporation, low-temperature chemistry, and the ignition process. A buffer zone of three cells, as depicted in Fig. 1(b), is maintained around the spray to ensure that all of the necessary physical and chemical calculations occur within the refined region. With all refinement stages, the total mesh count varies from approximately 9.5 million cells at initialisation to 36 million as the spray penetrates beyond 50 mm.

2.2.4. Spray and combustion modelling

The current study adopts the `coneCylinder injection` model [29,31] to define the injection process, which extends the standard two-dimensional `cone injection model` in OpenFOAM to a fully three-dimensional configuration. Each Lagrangian parcel contains both methanol and n-dodecane components and is injected through a single nozzle. The amount of each component within a parcel is determined by the prescribed mass fraction. The thermo-physical properties of the fuel blends, including density (ρ) and specific heat capacity (c_p), are evaluated based on the mass fraction. At the same time, vapour pressure and diffusivity are computed from the mole fraction implemented within OpenFOAM. The mass flow rate is derived from the experimental data of Payri et al. [51] for n-dodecane. For methanol and n-dodecane/methanol blended cases, the mass flow rates are adjusted according to the density of the blends with respect to the mass flow rate of n-dodecane.

Following previous studies by Kaario et al. [52,53], the current study injects the droplet with a constant initial droplet diameter of

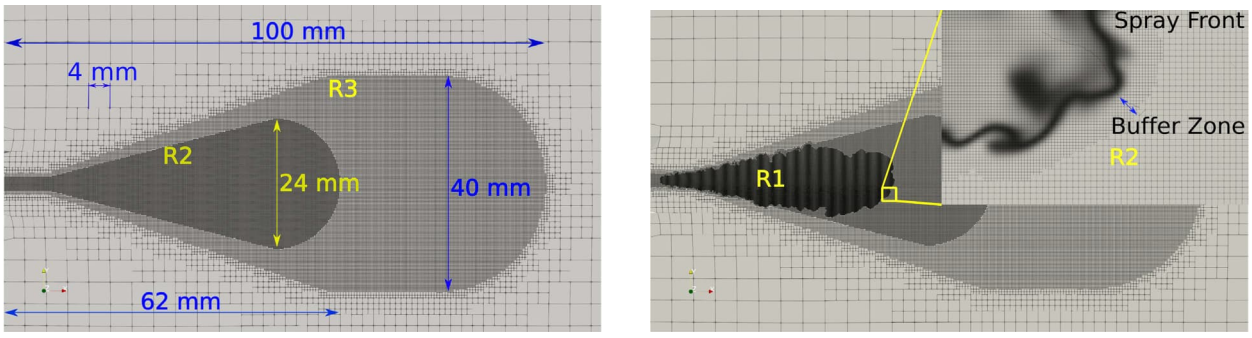

(a) Cut plane of the computational domain

(b) adaptive mesh refinement (AMR) refining the R2 region.

Fig. 1. A cut-plane view of the computational domain meshing, highlighting (a) the static refinement regions (R2 and R3) and (b) adaptive mesh refinement (AMR) (R1). R1, R2, and R3 correspond to 62.5 μm, 125 μm, and 250 μm respectively.

1 μm, corresponding to a Weber number (*We*) below 12. Under this condition, the study employs Lagrangian particle tracking (LPT) with a no-breakup model assumption under an implicit–LES (ILES) framework, since droplet breakup occurs for Weber number exceeding 12. Previous studies [31,54] have demonstrated that this approach in ILES reliably captures the key features of high-speed sprays at engine-relevant conditions. Additionally, the current study adopts the Ranz–Marshall correlation [55] with Bird's correction models for heat transfer, the `liquidEvaporationBoil` [56] for phase change, while the `sphereDrag` model governs the droplet motion and aerodynamic drag effects.

The current study employs `DLBFoam` [57–59] to compute the chemical source terms: filtered species reaction rates ($\overline{\omega_k}$) and heat release rate (HRR) ($\overline{\omega_h}$) in Eqs. (3) and (4), respectively. Turbulent–chemistry interactions (TCI) are treated using a first-order closure hypothesis, i.e., $\overline{\omega_k} = \omega_k(\tilde{Y}_i, \tilde{T}, \overline{p})$. No sub-grid scale model is adopted for the chemical source terms in the equations. The underlying assumption is that the high turbulence associated with the spray injection leads to intense mixing, and the high mesh resolution and the direct chemistry integration capture the broadened reaction zone chemistry, leading to a sufficient solution to the reacting problem. [41].

For chemical kinetics, the study adopts a mechanism developed by Frassoldati et al. [60] (hereafter referred to as `Polimi96`) with two additional species, N and NO, along with extended Zeldovich reactions [61,62]. The corresponding Arrhenius parameters are taken from [63–65]. The resulting mechanism is denoted as the `modified-Polimi`. The original Polimi96 comprises 96 species and 993 reactions, and has been validated for n-dodecane combustion by Kahila et al. [41] and Tekgul et al. [30].

Additionally, the study compares the NO emissions predicted by the modified-Polimi mechanism with an established mechanism for n-dodecane, methanol, and NO_x chemistry, developed by CRECK Modelling Group (hereafter referred to as `detailed-CRECK`, `TOT_HT_LT_NOX_537_18250`) [66–70]. The comparison of NO emission predicted by the two mechanisms are presented in the supplementary materials (Section 1).

3. Experimental data and validation of the spray model

3.1. Validation of pure n-dodecane spray flame

This section validates the spray model for pure n-dodecane against the existing ECN Spray A and Spray D datasets under both non-reacting and reacting conditions [43–46]. The validation includes liquid and vapour penetration and ignition delay time (IDT, $\tau_{2,LES}$) for both sprays, with ensemble and radial averaged mixture fraction and flame lift–off length (FLOL) for Spray A. The liquid penetration length follows the ECN definition [71] as the farthest axial location, where the projected liquid volume (PLV) equals 0.2×10^{-3} mm^3 liquid mm^{-2}. The PLV represents the ratio of the volume of the sprayed liquid to the projected area of the liquid. Vapour penetration is the axial position where the fuel mass fraction first reaches 0.1%. The IDT ($\tau_{2,LES}$) is the time of maximum temperature gradient ($\max(dT_{\max}/dt)$), while the FLOL denotes the first axial location where the OH radical concentration reaches 2% of maximum ($OH_{\max}$). The details on the experimental setup and the validation results are presented in the Supplementary materials (Section 2 and 3, respectively).

3.2. Validation of pure methanol spray flame

Here, we present the validation for pure methanol spray under the Spray D condition mentioned in Table 1. The validation is performed with new experimental data from the Spray Combustion Laboratory at Sandia National Laboratory [47]. Fig. 2 provides the validation results for pure methanol sprays under both reacting and non-reacting conditions, against the Spray D measurements. The validation dataset includes liquid and vapour penetration measurements under non-reacting conditions at 1000 K, and IDT ($\tau_{2,LES}$) and flame lift–off length (FLOL) under reacting conditions at 1100 and 1200 K, and 15% O_2. The definition of liquid and vapour penetration length, FLOL, and IDT, remains unchanged from the validation of n-dodecane in Section 3.1.

The simulated vapour penetration profiles in Fig. 2(a) demonstrate good correspondence with the experimental measurements, while the simulated liquid penetration exhibits a slight underprediction by approximately 2 mm. Figs. 2(b) and 2(c) compares the simulated and experimental values for IDT and FLOL at 1100 and 1200 K, and 15% O_2. The blue bars in the figures delineate the standard deviation in the experimental observations. The simulated IDT values are 1.1 and 0.33 ms at 1100 and 1200 K, compared to experimental values of 0.78 ± 0.47 ms and 0.28 ± 0.09 ms, respectively. The corresponding simulated FLOL values are 21 and 14 mm, compared to the measurements of 26 ± 6 mm and 13 ± 4 mm, respectively. A coarse mesh of 125 μm is employed to calculate FLOL at 1100 K, while a fine mesh of 62.5 μm has been adopted for the remaining calculations.

In summary, the simulated value at 1100 K for IDT and FLOL deviates by approximately 40% from the mean experimental observation but remains within the experimental uncertainty range, indicating that the discrepancies are not statistically significant. Overall, the results confirm the model's ability to accurately capture the spray and ignition characteristics of methanol.

3.3. Ignition delay of methanol/n-dodecane blends: comparison with the CRU experiments

This section compares the IDT ($\tau_{2,LES}$) predicted by the LES simulations of the methanol/n-dodecane blends with new, previously unpublished experimental data from the Combustion Research Unit

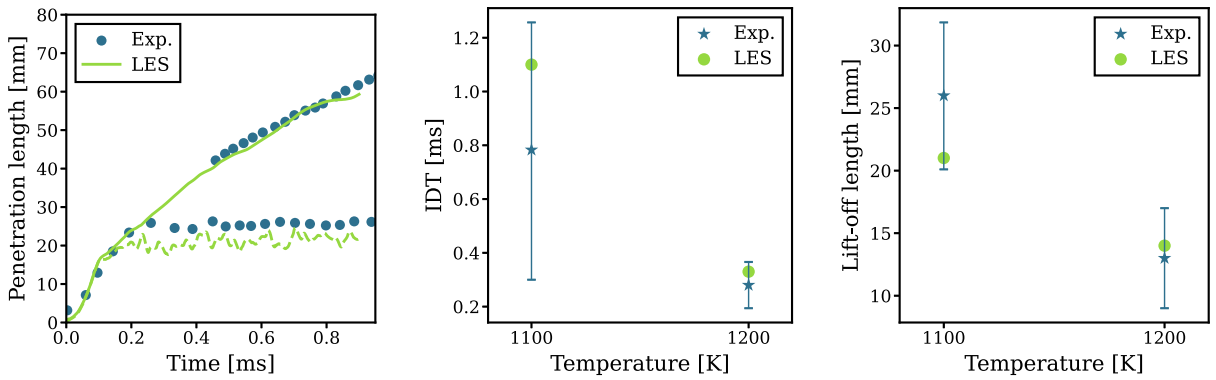

(a) Liquid and vapour penetration (b) Ignition delay time (IDT, $\tau_{2,LES}$) [ms] (c) Flame lift-off length (FLOL) [mm]

Fig. 2. Validation of the simulation results for methanol spray against experimental data - (a) Liquid and vapour penetration at 1000 K, (b) Ignition delay time (IDT, $\tau_{2,LES}$) at 1100 and 1200 K, and (c) Flame lift-off length at 1100 and 1200 K – under Spray D conditions. The blue bars in sub-Figures b and c illustrate the standard deviation in the experimental observation.

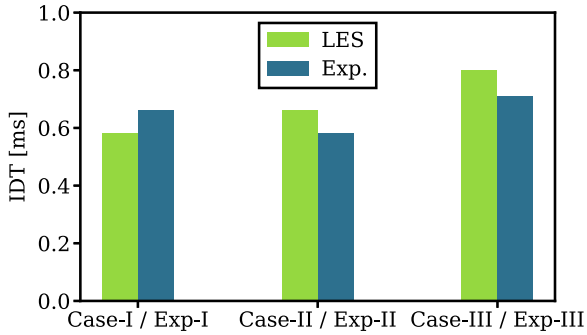

Fig. 3. Comparison of ignition delay time (IDT) of methanol/n-dodecane blends from the LES with the Combustion Research Unit (CRU) experiments. The definitions of the CRU experimental cases (Exp-I, Exp-II, and Exp-III) are provided in Table 1, while the LES cases – Case-I, Case-II, Case-III – refers to 0% methanol, 90% n-dodecane at 900 K, 20%–80% at 950 K, and 30%–70% at 1000 K, respectively, and are elaborated in Table 2.

(CRU) [26], and presented in Fig. 3. The experiments and simulations define the IDT as the time when the pressure rise reaches 0.1 bar. Details of the experimental setup are discussed in the supplementary materials (Section 4).

Some differences exist between the experimental and simulation conditions. The ambient pressure and temperature vary by 0.6 to 0.8 MPa and 20 K, respectively. The injection pressure for the experiments was recorded at 100 MPa, while that of the simulation corresponds to 150 MPa. The experiments employ octanol as a co-solvent to blend methanol and diesel, while the simulation does not include octanol. In the simulations, n-dodecane replaces the octanol fraction used in the experiments. Shock-tube studies by Cai et al. [72] and Shao et al. [73] reported that n-dodecane and octanol exhibit similar ignition delay time at the temperature range of the current study (900–1100 K). It is elaborated in the supplementary materials (Section 5). In addition, their thermo-physical properties are also comparable: for n-dodecane heat of vaporisation and specific heat capacity (c_p) (65 kJ mol^{-1}, 375 J mol^{-1} K^{-1} at 300 K) are similar to those of octanol (70 kJ mol^{-1}, 320 J mol^{-1} K^{-1} at 300 K). Due to these similarities, substituting octanol with n-dodecane in the simulations is considered to have a low influence on the predicted ignition delay. Nevertheless, the detailed combustion chemistry of octanol differs from that of n-dodecane. This aspect lies beyond the scope of the present study and requires further investigation.

The IDT values obtained from the experimental and LES results demonstrate a very close agreement, despite the small differences in the setups. The CRU experiments provide a valuable comparison for the LES simulations, as experimental data on these blends are rare in literatures. However, more data, such as liquid and vapour penetration, and flame lift–off length (FLOL) are required for a more comprehensive validation.

4. Results and discussion

4.1. 0–D analysis

This section analyses of the variations of ignition delay time (IDT) – obtained from 0–D simulations ($\tau_{2,0d}$) – for different methanol/n-dodecane blending ratios at various ambient temperatures (900, 950, 1000, and 1100 K) as well as the mixture fraction (Z), illustrated in Fig. 4. The fuel blending ratios vary from 100% methanol/0% n-dodecane (yellow line in the figure) to 0% methanol/100% n-dodecane (blue line in the figure). The figures also highlight the most reactive mixture fraction (Z_{MR}, indicated by ★) and the stoichiometric line (marked by the black dashed line), which separates the rich and lean regions. Here, the most reactive mixture fraction (Z_{MR}) corresponds to the minimum IDT (IDT_{MR}) for each blending ratio.

Fig. 4 illustrates the low-temperature reactivity of methanol and the strong temperature sensitivity of methanol combustion, consistent with previous literature [15,19,22,33,74]. In the figure, IDT_{MR} increases correspondingly to methanol, whereas IDT_{MR} decreases sharply with increasing ambient temperature. A noteworthy observation near 80%–100% methanol at 1100 K (Fig. 4(d)), at first glance, the IDT_{MR} value seems to decrease with increasing methanol percentage. This would suggest that the addition of methanol results in a higher reactivity at high temperature. However, a similar analysis with the detailed-CRECK mechanism displays that a higher content of methanol inhibits the reaction of the mixture even at 1100 K. Details on the sensitivity analysis of the mechanism and its impact on the IDT values are discussed in the supplementary materials (Section 6).

Kaario et al. [22] demonstrated that methanol tends to ignite on the lean side of the mixture, whereas n-dodecane ignites on the rich side. Fig. 4 reveals a similar behaviour, as with an increase in methanol content, the most reactive mixture fraction shifts from the rich region to the lean. The figures indicate that the transition of the most reactive mixture fraction from rich to lean area occurs between approximately 75% and 90% methanol, where two local minima in the IDT appear.

This analysis assists in evaluating promising methanol/n-dodecane blends at various temperatures that exhibit a reasonable IDT with

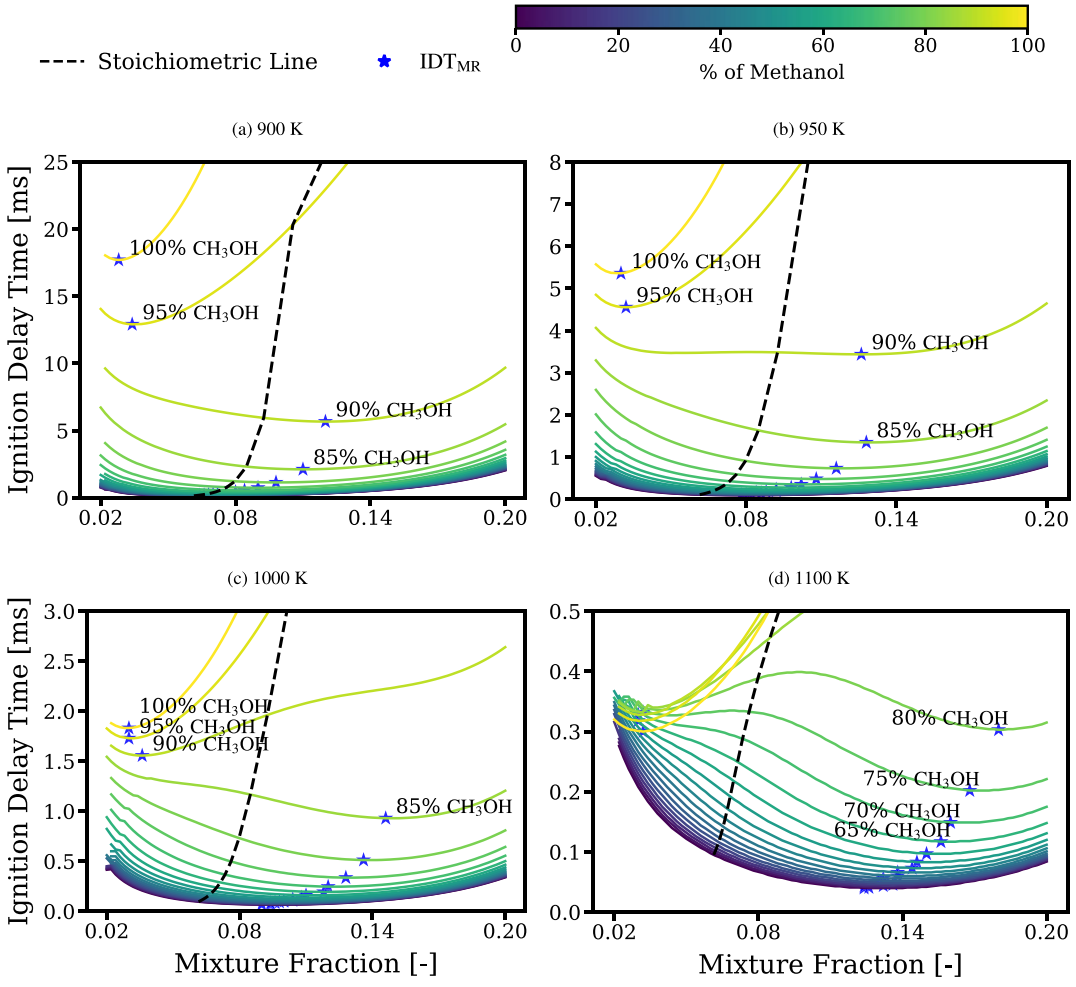

Fig. 4. Mixture fraction (Z) vs. ignition delay time (IDT) from the mixing-line concept using 0D homogeneous-reactor calculations with the modified Polimi chemical kinetics mechanism at different ambient temperatures, highlighting the most reactive IDT (IDT$_{MR}$).

engine-relevant time scales (IDT < 1 ms) under LES conditions. Studies [33,75,76] reported that for n-dodecane spray, the IDT in three-dimensional LES ($\tau_{2,LES}$) is approximately two to three times the IDT obtained in 0D ($\tau_{2,0d}$) at 950 and 1000 K. Similarly, Kaario et al. [22] observed that for pure methanol at 1100 K, $\tau_{2,LES}$ corresponds to 4.18 times the $\tau_{2,0d}$. Based on these findings, the present study selects LES cases with the assumption that for sprays with a high percentage of n-dodecane, $\tau_{2,LES}$ is three times larger than $\tau_{2,0d}$, while for sprays with a high methanol content, $\tau_{2,LES}$ is four times longer than $\tau_{2,0d}$.

4.2. LES simulations

4.2.1. Ignition analysis of 3D flames using LES technique

Following the 0–D simulations and presenting the validation results, potential blends were screened based on the ignition criteria ($\tau_{2,LES}$ < 1 ms). From the screening process, four blending ratios – one for each ambient temperature (900, 950, 1000, 1100 K) – are selected for LES analysis. It should be noted that several LES cases were initially considered for each temperature. However, preliminary simulations with a coarse mesh indicated that the mixtures listed in Table 2 represent the maximum methanol fraction at a particular ambient temperature that satisfies the ignition criteria. 10% additional methanol in any case would result in ignition exceeding 1 ms.

The analysis of $\tau_{1,LES}$ and $\tau_{2,LES}$ in Table 2 indicates that increasing the methanol fraction prolongs $\tau_{2,LES}$, even at high ambient temperatures. In LES, we define IDT or ($\tau_{2,LES}$) as the time when the pressure rise is 0.1 bar. At 900 K, methanol replaces only 10% of n-dodecane and yields $\tau_{2,LES}$ of 0.58 ms (case I). As the temperature rises to 950 and 1000 K, substitution levels of 20% and 30% n-dodecane with methanol produce IDT of 0.65 and 0.8 ms (case II and case III), respectively. At 1100 K, methanol replacement reaches 70%, with τ_2 increasing to 0.99 ms (case IV). Figs. 5 and 6 illustrate the combustion evolution of methanol/n-dodecane blends for cases I to IV at the ignition ($\tau_{2,LES}$) and quasi steady-state ($2 \times \tau_{2,LES}$) time instances, respectively.

Previous literature [41,42,50] classifies the spray combustion process into the following regions: (1) liquid core with rapid atomisation, evaporation, and mixing region, (2) low–temperature combustion (LTC) zone (3), transition to high–temperature combustion (HTC) (ignition), and (4) HTC zone. The regions are highlighted as A, B, C, and D, respectively, in Figs. 5 and 6. In the figures, the blue field delineates the methanol/n-dodecane fuel, highlighting the evaporation phase. The green and red–yellow field represents the LTC and HTC zones in the spray, respectively. The stoichiometric line – depicted as the yellow and black contour line in Figs. 5 and 6, respectively – separates the rich and lean regions of the spray. α is the ratio of the mass fraction of methanol (Y_{CH_3OH}) to the total mass fraction of the fuel blend ($Y_{CH_3OH} + Y_{C_{12}H_{26}}$). The current study defines the stoichiometric ratio as the point where the Bilger mixture fraction (Z) [77] equals the stoichiometric mixture fraction (Z_{st}).

The initiation of LTC, often referred to as the first-stage ignition (τ_1), produces several intermediate species. The LTC of n-dodecane produces species such as the dodecyl-peroxy radical ($C_{12}H_{25}OO$) [78,79] and formaldehyde (CH_2O) [80]. Similarly, methanol combustion emits CH_3O, CH_2O, and CH_2OH [10,81]. Since both fuels generate CH_2O

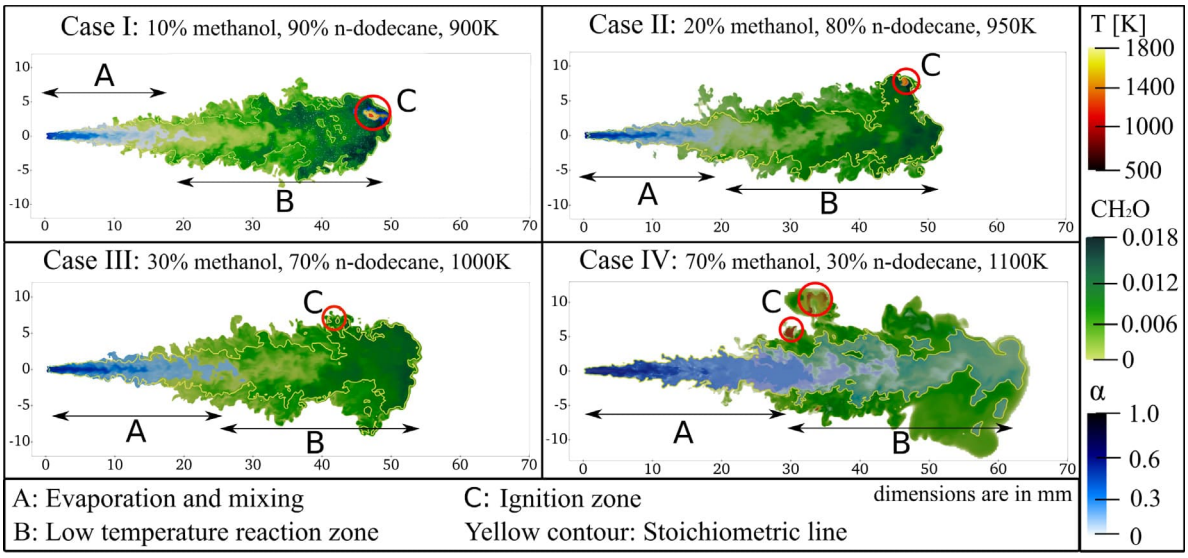

Fig. 5. The different phases of the ignition process for all cases at ignition delay time (IDT), highlighting the evaporation phase (A), low–temperature combustion (B), and ignition (C). The red circular inset (C) illustrates the ignition location. α is the ratio of the mass fraction of methanol to the total mass fraction of the fuel blend.

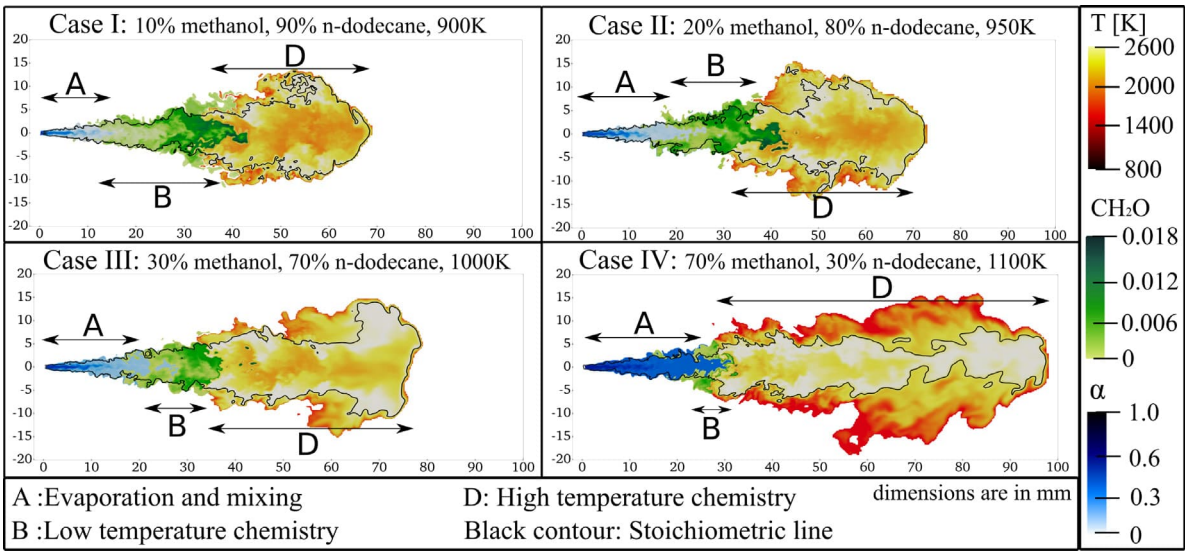

Fig. 6. The different phases of the flame development for all cases at quasi steady-state ($2 \times IDT$), highlighting the evaporation phase (A), low–temperature combustion (B), and high–temperature combustion (D). α is the ratio of the mass fraction of methanol to the total mass fraction of the fuel blend.

during LTC, the present study defines the first-stage ignition (τ_1) as the time when the spatially averaged CH_2O mass fraction reaches 20% of the maximum ($Y_{CH_2O_{max}}$) in the domain.

Fig. 5 highlights the presence of higher concentration of methanol in the spray core for all cases. This can be attributed to heat of vaporisation of methanol. In addition, the figure presents the ignition initiation location in the spray, labelled as *C*. For case IV, with predominantly methanol (70% [w]), the spray ignition occurs in the lean area of the spray compared to other cases, while for cases I and II with primarily n-dodecane, the spray ignition initiates from the rich region of the spray. For case III, the ignition starts near the stoichiometric line.

Fig. 6 provides a qualitative analysis of the flame development at quasi steady-state (2 × IDT). The figure highlights the evaporation phase (A), the LTC (B), and the HTC (D) zones. The spatial separation between the evaporation phase and the HTC region qualitatively indicates the flame lift–off length (FLOL) of the spray. During the HTC stage (Fig. 6), intermediate species such as CH_2O are consumed to form high-temperature species, like OH, resulting in a reduced area of the LTC region compared to the ignition stage. AS shown in Fig. 6, increasing the methanol percentage in the blend results in a progressive decrease in the area of the LTC region.

Fig. 7 presents the centreline temperature as a function of time for all cases. A higher centreline temperature for case IV (Fig. 7(d)) compared to case I, (Fig. 7(a)) can be observed. Temperature fluctuations along the centreline due to methanol are also evident. The figure additionally illustrates the temporal evolution of the FLOL.

4.2.2. *Temporal evolution of the 3D flames*

Next, we look into the temporal evolution of temperature and species such as CH_2O and OH in Fig. 8. In the figure, the first-stage ignition ($\tau_{1,LES}$) and the second-stage ignition ($\tau_{2,LES}$) are marked by ● and ★, respectively, with corresponding values listed in Table 2. The figure reveals that the methanol dominant blend (case IV) yields the highest concentration of CH_2O and OH species. However, the formation rate of CH_2O in case IV is slower than in cases I–III. Cases I–III show

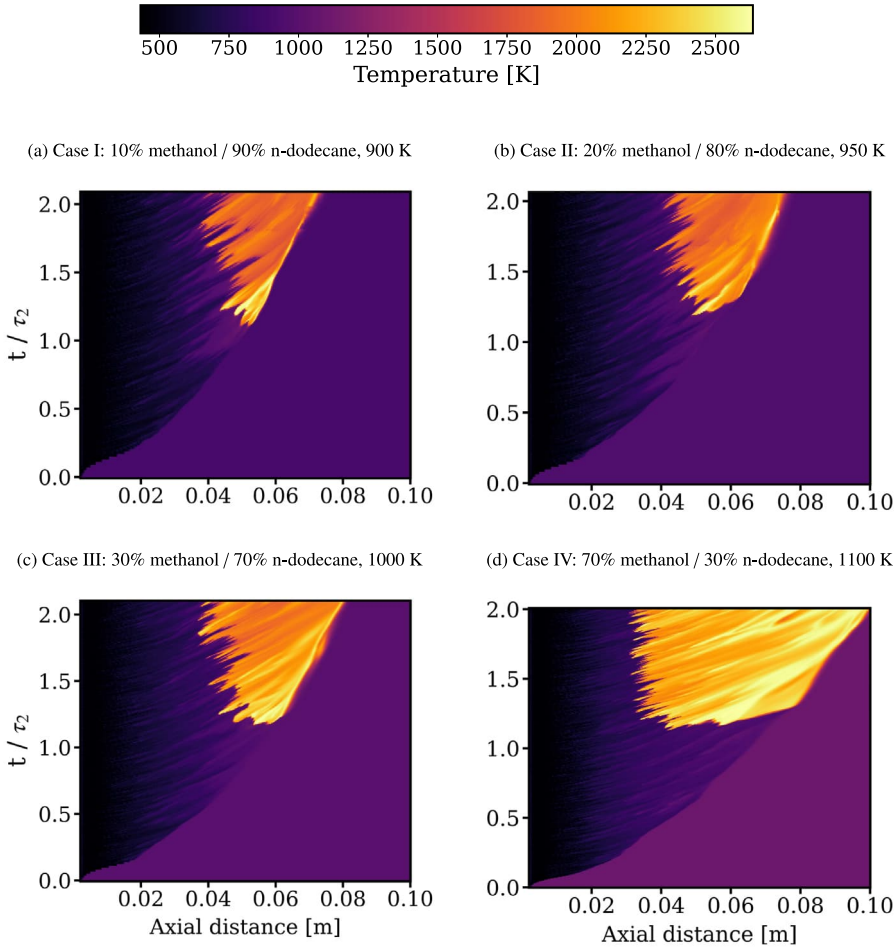

Fig. 7. Temporal evolution of centreline temperature of the methanol/n-dodecane blends.

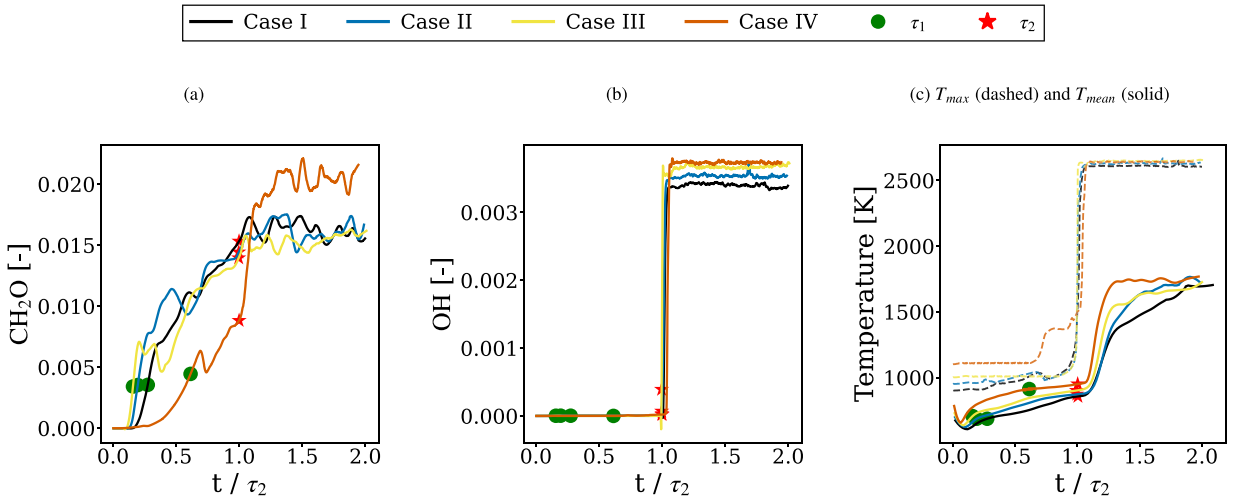

Fig. 8. Temporal evolution of maximum mass fraction of (a) CH_2O, (b) OH, and (c) maximum temperature (dashed) and mean spray temperature (solid) for $Z > 1 \times 10^{-3}$ in methanol/n-dodecane blends. The first-stage ($\tau_{1,LES}$) and the second-stage ignition ($\tau_{2,LES}$) are also highlighted.

comparable maximum CH_2O concentrations, ranging from 0.015 to 0.017.

The mean spray temperature (T_{mean}, depicted as a solid line) in Fig. 8(c), displays an initial decrease during the evaporation phase, occurring approximately 0.2 × IDT. Case IV exhibits the largest reduction in the average spray temperature ($\Delta T \approx 150$ K) compared to 116, 95, and 84 K for cases I, II, and III, respectively. Following the evaporation phase, the mean spray temperature gradually rises until

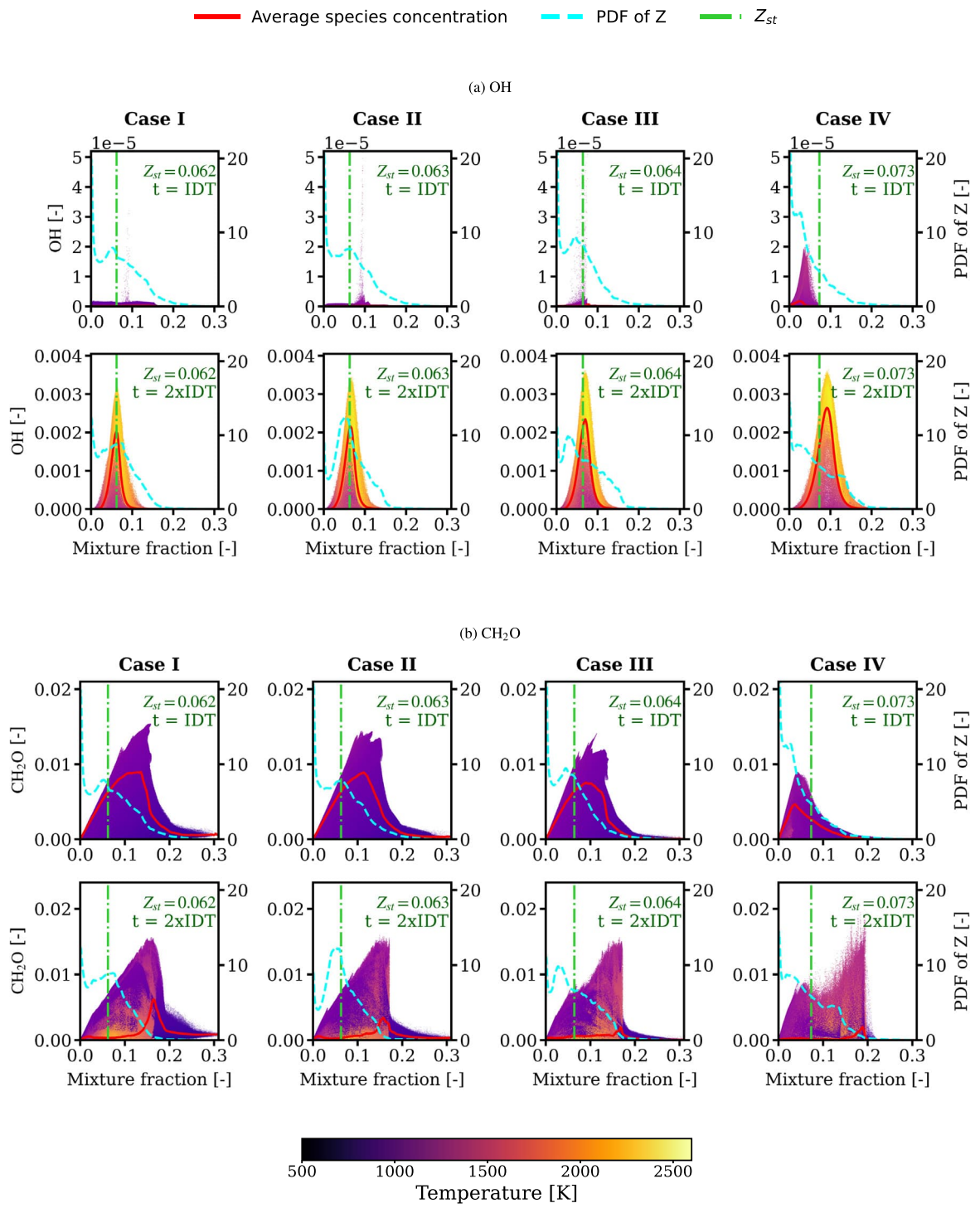

Fig. 9. Spatial concentration evolution of (a) OH and (b) CH_2O ($Z > 1 \times 10^{-3}$) at ignition and quasi steady-state (2 × IDT) instances. The colour of the scatter plots indicates the temperature corresponding to each mixture fraction. The red, green and cyan line represents the average species concentration, stoichiometric mixture fraction (Zst), and the probability distribution function (PDF) of the mixture fraction (Z), respectively.

ignition, after which the temperature increases rapidly and reaches a quasi steady-state. These observations highlight the reaction-inhibiting nature of methanol and the two-stage ignition process of methanol/n-dodecane blends.

Fig. 8(c) also depicts the temporal evolution of maximum temperature (T_{max}, depicted as a dashed line) in the domain. In all cases, the maximum temperature reaches approximately 2600 K. For the methanol-dominant blend (case IV), the T_{max} increases slightly during 0.8 × IDT then remains constant until ignition occurs. Cases I and II depict a similar trend around 0.7 × IDT, although the increase is less prominent compared to case IV.

4.2.3. Spatial evolution of the 3D flames

We now examine the spatial evolution of species and temperature with respect to mixture fraction ($Z > 1 \times 10^{-3}$). The scatter plot in Figs. 9(a) and 9(b) illustrates the spatial distribution of OH and CH_2O, for all cases, at ignition and at quasi steady-state (2 × IDT). The colour scale represents the temperature associated with the species at

Table 3
Sub-grouping the total heat release rate (HRR) by chemistry modes for methanol/n-dodecane blended fuel. The critical threshold values are $T_{cr} = 1250$ K, $CH_2O_{cr} = 2 \times 10^{-3}$, $H_2O_{2,cr} = 2 \times 10^{-4}$ and $OH_{cr} = 1 \times 10^{-5}$.

Group name	Definition	Colour
early LTC	$(CH_2O \geq 2\times10^{-6}) \cap (H_2O_2 < H_2O_{2,cr}) \cap (T < T_{cr})$	
LTC	$(CH_2O \geq 2\times10^{-6}) \cap (H_2O_2 \geq H_2O_{2,cr}) \cap (T < T_{cr})$	
pre-HTC	$(CH_2O < CH_2O_{cr}) \cap (H_2O_2 \geq H_2O_{2,cr}) \cap (T < T_{cr})$	
HTC pre-Ignition	$(OH < OH_{cr}) \cap (T \geq T_{cr})$	
HTC	$(OH \geq OH_{cr}) \cap (T \geq T_{cr})$	

a given mixture fraction (Z). The green dashed-dot line indicates the stoichiometric mixture fraction (Z_{st}) for the mixture, while the red solid line indicates the average of the scatter plot across the mixture fraction. The cyan dashed curve represents the probability distribution function (PDF) of the mixture fraction.

At ignition, the OH plots (top row in Fig. 9(a)) demonstrate that for cases I and II, the OH species form at mixture fraction of $Z = 0.093$ and $Z = 0.095$, with stoichiometric mixture fraction $Z_{st} = 0.062$ and $Z_{st} = 0.063$, respectively. The formation of OH coincides with the high-temperature flame region. This indicates that the flame initiates from the rich conditions of the spray. In contrast, for case IV, OH forms at the lean side at $Z = 0.028$ ($Z_{st} = 0.073$). For case III, OH forms near the stoichiometric mixture fraction.

Similarly, the majority of CH_2O species in case IV at IDT lie in the lean region of the spray, whereas for cases I–III, the majority of CH_2O lie in the rich regions. A slower development of the HTC in case IV, and higher mixing with the ambient, causes the CH_2O to shift to the lean condition.

At quasi steady-state (2 × IDT), Fig. 9(a) depicts an elevated temperature accompanied by higher OH, indicative of high-temperature flame formation. Case IV exhibits the higher average OH concentration (red solid line), compared to cases I–III. For cases I–III, at quasi steady-state, OH forms predominantly near stoichiometric conditions, while for case IV OH forms slightly towards the richer side. This trend is consistent with the qualitative observations from Figs. 6 which show higher temperatures closer to the spray core.

In contrast, at quasi steady-state, CH_2O (Fig. 9(b)) is consumed and exhibits a lower average concentration (red solid line) compared to the IDT. Nevertheless, the peak CH_2O concentration in the scatter plot increases for case IV at quasi steady-state relative to IDT. At IDT, the maximum CH_2O concentration is 0.009 at $Z = 0.04$, whereas at quasi steady-state it increases to 0.02 at $Z = 0.2$. The shift in mixture fraction associated with the maximum CH_2O concentration indicates that CH_2O formation becomes confined to smaller regions located closer to the spray core. Fig. 6 (case IV) further illustrates the location of the elevated CH_2O concentration (highlighted in dark green), which appears just upstream of the flame lift-off location.

The probability distribution function (PDF) of the mixture fraction (Z) for $Z > 1 \times 10^{-3}$ provides further insight into the mixture fraction evolution. The area under the cyan dashed curve indicates the probability of the mixture fraction in the domain. For cases I and II, the mixture distribution remains approximately balanced between rich and lean regions at both ignition and quasi steady-state. However, for cases III and IV, the lean region constitutes 60% and 74% of the total spray area at ignition, and 52% and 58% at quasi steady-state, respectively.

4.2.4. Heat release rate analysis

This section analyses the heat release rate (HRR) from all LES cases. The modelling method is described in Section 2.2.4. Following previous studies [22,29,33], the current work categorises the total HRR into 5 sub-groups: (1) early low–temperature combustion, (2) low–temperature combustion (LTC), (3) pre-high-temperature combustion, (4) high-temperature combustion pre-Ignition and (5) high–temperature combustion (HTC). The criteria for the subdivisions are summarised in Table 3.

Fig. 10 depicts the contributions of each subgroup to the total HRR. For all cases, the HTC contributes the highest (at least 80%) to the total HRR. Fig. 10 outlines that the HTC heat release at IDT reaches 1290 and 1150 kW for cases IV and III, respectively, while cases II and I yield 930 and 710 kW. The higher HTC in case IV can be attributed to the presence of a higher quantity of fuel/air mixture in the chamber at ignition. At quasi steady-state, the HTC decreases to approximately 300–400 kW for all cases.

Fig. 10 further describes that increase in methanol fraction suppresses the overall contribution of LTC to the total HRR. The share of LTC decreases from 16% to 8.3% as the methanol percentage increases from 10% to 70%, respectively. Additionally, the time when LTC starts also prolongs with an increase in methanol content. For cases I–III, the initiation of LTC chemistry starts from 0.3 × IDT, which peaks at 70 kW, 80 kW and 100 kW, respectively during ignition. However, for case IV (Fig. 10(d)), the LTC starts from 0.65 × IDT and reaches 120 kW near the IDT. In addition, at quasi steady-state for cases I–III, the LTC stabilises at 30–40 kW, whereas for case IV the LTC decreases to 4.5 kW.

4.2.5. Emission analysis

This section evaluates the temporal evolution of emissions – NO, CO, and C_2H_2 (a soot precursor) – from the combustion of the methanol/n-dodecane blends, and presented in Fig. 11. In addition, it examines the formation of NO as a function of mixture fraction (Z) and the corresponding temperature, and is illustrated in Fig. 12.

Due to the elevated ambient temperature in case IV, the NO emissions are 2.5 times higher than in case I, and the NO emission decreases with a reduction in the ambient temperature, and depicted in Fig. 11(a). Fig. 11(c) illustrates that C_2H_2 emissions in case IV are 2.2 times lower compared to case I. Across cases I–III, the C_2H_2 concentration reaches roughly 0.022 at quasi steady-state, though for case III, the generation rate is slower compared to cases I and II, but it attains a comparable concentration at quasi steady-state. The generation rate and maximum concentration of CO are similar across all cases, as presented in Fig. 11(b).

Fig. 12 presents the spatial distribution of NO as a function of mixture fraction (Z) at quasi steady-state (2 × IDT). The colour bar and green dashed line indicate the temperature and stoichiometric mixture fraction (Z_{st}), respectively. For case IV, NO species forms on the richer side and closer to the spray core, while for cases I–III, the formation occurs at stoichiometric conditions. The peak of NO formation coincides with the higher temperature region in the spray.

Overall, the NO emissions from the `modified Polimi` mechanism have been compared with those from the `detailed-CRECK` mechanism in 0-D analysis and elaborated in supplementary materials (Section 1), which exhibit good agreements. The formation of NO in the combustion of methanol/n-dodecane blends occurs mostly through thermal NO pathways and therefore displays a strong temperature sensitivity.

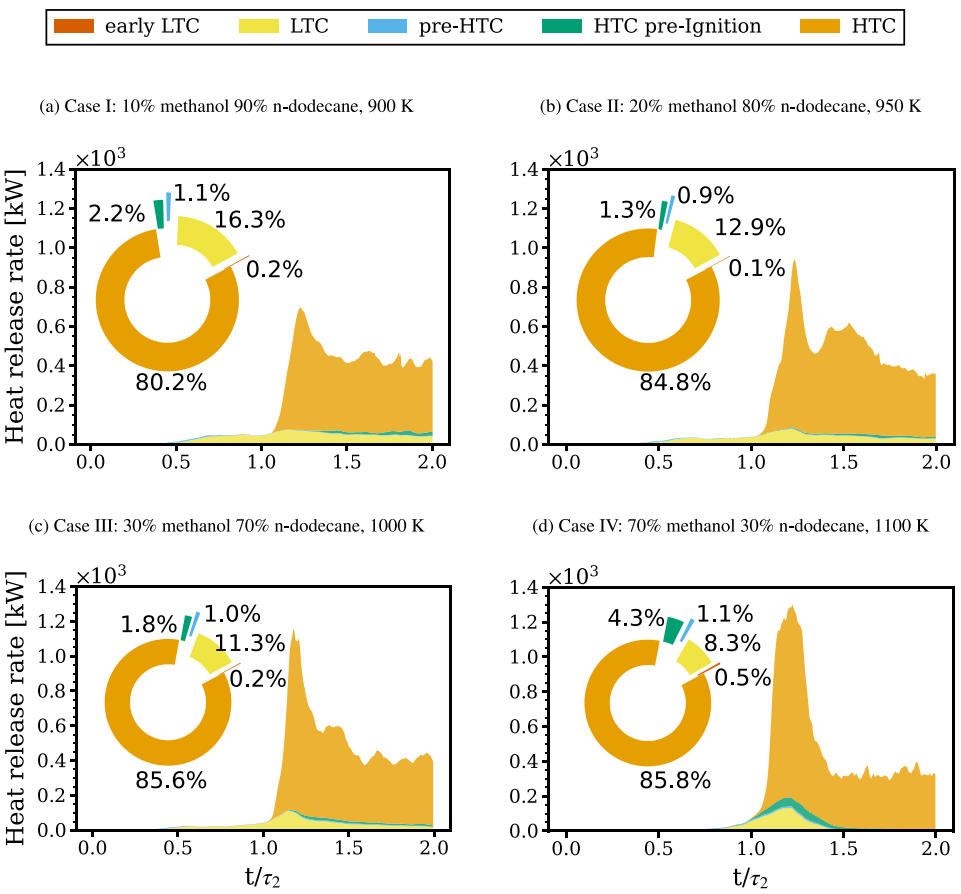

Fig. 10. Volume integrated total heat release rate (HRR) of the entire spray as a function of normalised time. The pie chart illustrates the cumulative HRR contributions over the spray duration.

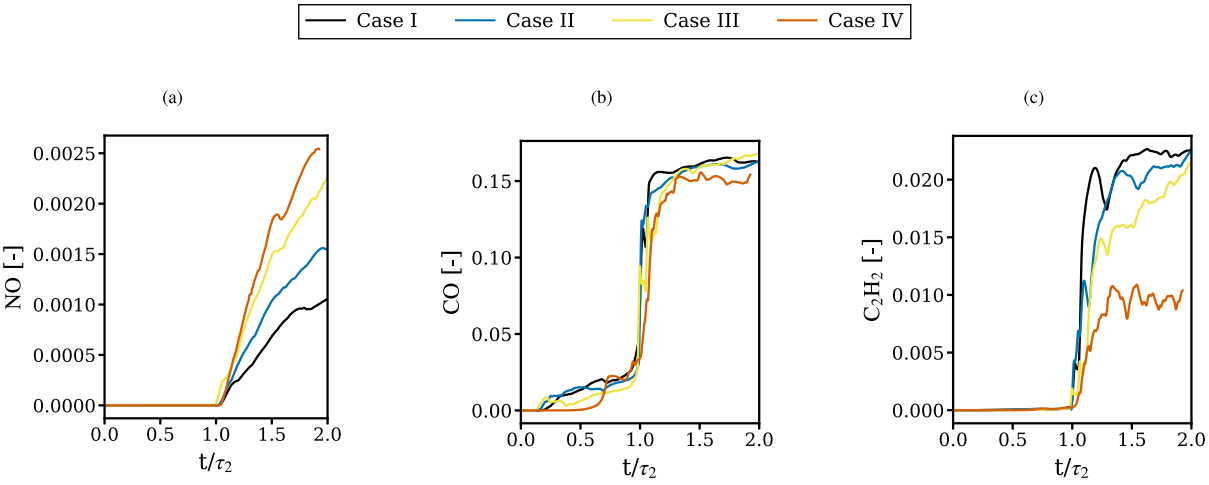

Fig. 11. Temporal evolution of maximum emissions concentration: (a) NO, (b) CO, and (c) C_2H_2 for all cases.

5. Conclusion and future work

The present study investigated the reacting spray behaviour of methanol/n-dodecane blends over a range of mixing ratios and ambient temperatures employing the large eddy simulation (LES) technique in OpenFOAM. The primary objective was to quantify the maximum methanol fraction in the blend that ensures complete combustion within the engine-relevant ignition delay time (IDT) < 1 ms. The modified Polimi mechanism (the `Polimi96` mechanism with extended Zeldovich reactions) was employed for chemical kinetics. The main conclusions are summarised as follows:

1. The validation of the spray model for pure methanol and n-dodecane under reacting and non-reacting conditions was successful.
2. The IDT from the Combustion Research Unit (CRU) measurements exhibited good correspondence with the methanol/n-dodecane blend LES cases.

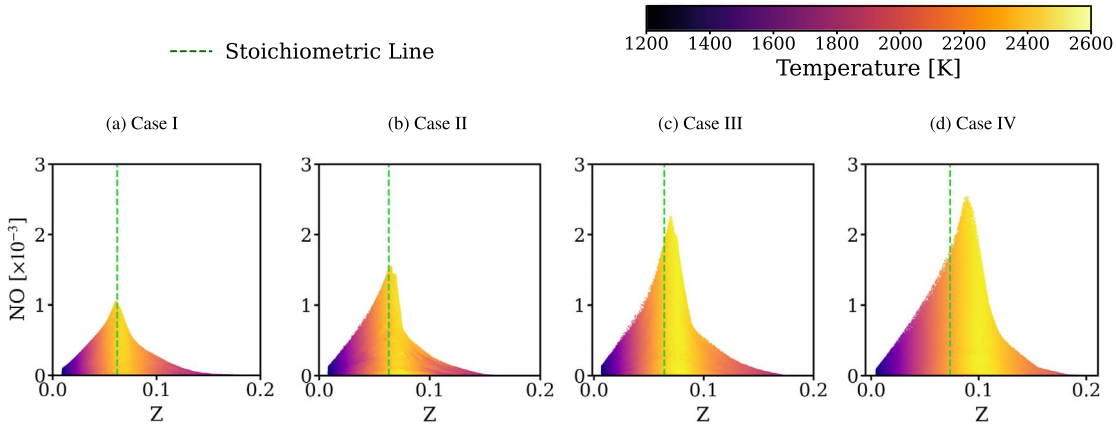

Fig. 12. Mass fraction of NO as a function of mixture fraction (Z) for all cases at quasi steady-state. The colour bar and dashed line highlight the corresponding temperature [K] and stoichiometric line (Z_{st}).

3. Four cases at different temperatures met the ignition criteria (IDT < 1 ms):

   (I) 10% methanol, 90% n-dodecane at 900 K
   (II) 20% methanol, 80% n-dodecane at 950 K
   (III) 30% methanol, 70% n-dodecane at 1000 K
   (IV) 70% methanol, 30% n-dodecane at 1100 K

   An additional 10% increase in the methanol content in any of the cases led to the IDT exceeding 1 ms.
4. The addition of methanol content inhibits the ignition process of the blend, as the higher heat of vaporisation of methanol results in a larger drop in mean spray temperature during the evaporation phase. In addition, net consumption of OH at low temperature from methanol combustion further hinders the overall ignition process of the blend.
5. The methanol-dominant blend (case IV) exhibited the shortest flame lift–off length of 26.04 mm, while the remaining cases showed longer values ranging between 29 and 30 mm.
6. For the methanol-dominant blend (case IV), the ignition takes place on the lean side of the spray (Z = 0.028 with Z_{st} = 0.073), whereas for cases I and II reactions occur on the rich side (Z = 0.093 and Z = 0.095 with Z_{st} = 0.062 and Z_{st} = 0.063, respectively). For case III, the spray ignition occurs near the stoichiometric ratio (Z = 0.07 with Z_{st} = 0.064).
7. The methanol-dominant blend (case IV) displayed the highest heat release from high-temperature combustion (HTC) of 1290 kW during ignition, whereas cases I, II, and III exhibited 710, 930, and 1150 kW, respectively. The higher heat release in case IV can be attributed to a greater presence of fuel/air mixture in the chamber at ignition. At quasi-steady state, the total heat release decreases to approximately 300–400 kW for all cases.
8. The contribution of low–temperature combustion (LTC) to the total heat release rate decreases with an increase in methanol percentage. For cases I to IV LTC contributed 16.3%, 12.9%, 11.3%, and 8.3% to the total heat release rate, respectively.
9. In the LES simulations, the methanol-dominant blend (case IV) exhibited the highest centreline temperature, while the averaged spray temperature remained similar across all cases.
10. The higher centreline temperature in methanol-rich blend (case IV) resulted in the highest NO and lowest soot precursor (C_2H_2) concentrations. In contrast, CO remains unchanged across all cases.

Given the novelty of this work, further validation of n-dodecane/methanol blends is required. Although IDT of the blends were compared with the measurements from the CRU, additional parameters such as liquid and vapour penetration and flame lift–off length are required for a complete validation. Moreover, the development of a reasonably sized reaction mechanism that incorporates methanol, n-dodecane, and octanol will also be important for a fully representative simulation.

CRediT authorship contribution statement

Bishal Shrestha: Writing – original draft, Visualization, Methodology, Investigation, Formal analysis, Conceptualization. **Fatimoh Balogun:** Writing – review & editing, Investigation. **Kevin Wan:** Investigation. **Junghwa Yi:** Investigation. **Huaying Wang-Alho:** Investigation. **Shervin Karimkashi:** Writing – review & editing, Supervision, Conceptualization. **Katriina Sirvio:** Writing – review & editing, Resources, Project administration, Funding acquisition. **Julien Manin:** Writing – review & editing, Supervision, Investigation. **Maciej Mikulski:** Writing – review & editing, Resources, Project administration, Funding acquisition. **Jari Hyvönen:** Supervision, Project administration. **Ossi Kaario:** Writing – review & editing, Supervision, Funding acquisition, Conceptualization.

Declaration of competing interest

The authors declare that they have no known competing financial interests or personal relationships that could have appeared to influence the work reported in this paper.

Acknowledgements

The present study is part of the Flexible Clean Propulsion Technologies project (ref. 9719/31/2023), which is co-funded by Business Finland. Shervin Karimkashi would like to acknowledge the Research Council of Finland project Wet-HyAm (grant number 361479). The computational resources are provided by CSC-Finnish IT Center for Science. The pure n-dodecane and methanol experiments were performed at the Combustion Research Facility, Sandia National Laboratories in Livermore, CA. Sandia National Laboratories is a multi-mission laboratory managed and operated by National Technology & Engineering Solutions of Sandia, LLC (NTESS), a wholly owned subsidiary of Honeywell International Inc., for the U.S. Department of Energy's National Nuclear Security Administration (DOE/NNSA) under contract DE-NA0003525. This work was co-authored by an employee of NTESS. The employee retains shared ownership of the work and is solely responsible for its content. Any opinions expressed do not necessarily reflect the views of the U.S. Government. The U.S. Government retains a non-exclusive, irrevocable, worldwide license to reproduce or publish

this work, or to allow others to do so, for U.S. Government purposes. Public access to results of federally funded research will be provided in accordance with the DOE Public Access Plan.

Appendix A. Supplementary data

Supplementary material related to this article can be found online at https://doi.org/10.1016/j.fuproc.2026.108435.

Data availability

Data will be made available on request.

References

[1] K. Inagaki, T. Fuyuto, K. Nishikawa, K. Nakakita, I. Sakata, Dual-fuel PCI combustion controlled by in-cylinder stratification of ignitability, in: SAE 2006 World Congress & Exhibition, SAE International, 2006.

[2] S. Curran, V. Prikhodko, K. Cho, C.S. Sluder, J. Parks, R. Wagner, S. Kokjohn, R.D. Reitz, In-cylinder fuel blending of gasoline/diesel for improved efficiency and lowest possible emissions on a multi-cylinder light-duty diesel engine, in: SAE 2010 Powertrains Fuels and Lubricants Meeting, SAE International, 2010.

[3] K. Asfar, H. Hamed, Combustion of fuel blends, Energy Convers. Manage. 39 (10) (1998) 1081–1093.

[4] S. Pan, X. Liu, K. Cai, X. Li, W. Han, B. Li, Experimental study on combustion and emission characteristics of iso-butanol/diesel and gasoline/diesel RCCI in a heavy-duty engine under low loads, Fuel 261 (2020) 116434.

[5] C. Yao, C. Cheung, C. Cheng, Y. Wang, T. Chan, S. Lee, Effect of diesel/methanol compound combustion on diesel engine combustion and emissions, Energy Convers. Manage. 49 (6) (2008) 1696–1704.

[6] D.K. Soni, R. Gupta, Optimization of methanol powered diesel engine: A CFD approach, Appl. Therm. Eng. 106 (2016) 390–398.

[7] D. Güllü, A. Demirbaş, Biomass to methanol via pyrolysis process, Energy Convers. Manage. 42 (11) (2001) 1349–1356.

[8] S. Sollai, A. Porcu, V. Tola, F. Ferrara, A. Pettinau, Renewable methanol production from green hydrogen and captured CO_2: A techno-economic assessment, J. CO_2 Util. 68 (2023) 102345.

[9] T. Wang, T. Zhou, C. Li, M. Zhang, Q. Song, H. Yang, Biogas-to-methanol: A new green methanol production process based on anaerobic digestion of biomass, Energy Convers. Manage. 321 (2024) 119065.

[10] Z. Ming, B. Liu, X. Zhang, M. Wen, H. Liu, Y. Cui, Y. Ye, C. Wang, C. Jin, A.A. Yusuf, E.B. Agyekum, Study of methanol spray flame structure and combustion stability mechanisms by optical phenomenology and chemical kinetics, Fuel Process. Technol. 252 (2023) 107947.

[11] P.T. Aakko-Saksa, M. Westerholm, R. Pettinen, C. Söderström, P. Roslund, P. Piimäkorpi, P. Koponen, T. Murtonen, M. Niinistö, M. Tunér, J. Ellis, Renewable methanol with ignition improver additive for diesel engines, Energy & Fuels 34 (1) (2020) 379–388.

[12] C. Cheng, R. Faurskov Cordtz, T. Berg Thomsen, N. Langballe Førby, J. Schramm, Application of methanol with an ignition improver in a small marine CI engine, Energy Convers. Manage. 271 (2022) 116311.

[13] Z. Huang, H. Lu, D. Jiang, K. Zeng, B. Liu, J. Zhang, X. Wang, Combustion behaviors of a compression-ignition engine fuelled with diesel/methanol blends under various fuel delivery advance angles, Bioresour. Technol. 95 (3) (2004) 331–341.

[14] D. Qi, H. Chen, L. Geng, Y. Bian, X. Ren, Performance and combustion characteristics of biodiesel–diesel–methanol blend fuelled engine, Appl. Energy 87 (5) (2010) 1679–1686.

[15] A. García, J. Monsalve-Serrano, C. Micó, M. Guzmán-Mendoza, Parametric evaluation of neat methanol combustion in a light-duty compression ignition engine, Fuel Process. Technol. 249 (2023) 107850.

[16] N. Yilmaz, Comparative analysis of biodiesel–ethanol–diesel and biodiesel–methanol–diesel blends in a diesel engine, Energy 40 (1) (2012) 210–213.

[17] A.O. Hasan, A.I. Osman, A.H. Al-Muhtaseb, H. Al-Rawashdeh, A. Abu-jrai, R. Ahmad, M.R. Gomaa, T.J. Deka, D.W. Rooney, An experimental study of engine characteristics and tailpipe emissions from modern DI diesel engine fuelled with methanol/diesel blends, Fuel Process. Technol. 220 (2021) 106901.

[18] A. Ghosh, R. Ravikrishna, Evaporating spray characteristics of methanol-in-diesel emulsions, Fuel 290 (2021) 119730.

[19] J. Zhu, S. Wang, M. Raza, Y. Feng, J. Li, Y. Mao, L. Yu, Y. Qian, X. Lu, Autoignition behavior of methanol/diesel mixtures: Experiments and kinetic modeling, Combust. Flame 228 (2021) 1–12.

[20] Y. Wang, P. Dong, W. Long, J. Tian, F. Wei, Q. Wang, Z. Cui, B. Li, Characteristics of evaporating spray for direct injection methanol engine: comparison between methanol and diesel spray, Processes 10 (6) (2022) 1132.

[21] X. Wang, X. Chang, J. Liu, J. Gao, J. Wu, H. He, Experimental investigation of high-pressure methanol spray characteristics for engines, Appl. Therm. Eng. 271 (2025) 126388.

[22] O.T. Kaario, S. Karimkashi, A. Bhattacharya, V. Vuorinen, M. Larmi, X.-S. Bai, A comparative study on methanol and n-dodecane spray flames using large-eddy simulation, Combust. Flame 260 (2024) 113277.

[23] A.L. Delgado-Mejia, L.C. Olmos-Villalba, Heptane and dodecane as surrogates of diesel fuel, a comparison with Computational Fluid Dynamics (CFD), Rev. CINTEX 20 (1) (2015) 97–110.

[24] J. Yadav, S. Pischinger, A novel surrogate fuel approach for the numerical simulation of renewable fuels for the transport sector, Energy Convers. Manage. 287 (2023) 117056.

[25] L. Pickett, G. Bruneaux, R. Payri, Engine combustion network special issue, Int. J. Engine Res. 21 (1) (2020) 11–14.

[26] Fueltech Solutions AS, Combustion research unit (CRU) – Fueltech solutions, 2025, https://www.fueltechsolutions.com/cru. (Accessed: 31 October 2025).

[27] Z. Hu, L. Somers, T. Davies, A. McDougall, R. Cracknell, A study of liquid fuel injection and combustion in a constant volume vessel at diesel engine conditions, Fuel 107 (2013) 63–73.

[28] H. Weller, G. Tabor, H. Jasak, C. Fureby, A tensorial approach to computational continuum mechanics using object orientated techniques, Comput. Phys. 12 (1998) 620–631.

[29] H. Kahila, A. Wehrfritz, O. Kaario, M. Ghaderi Masouleh, N. Maes, B. Somers, V. Vuorinen, Large-eddy simulation on the influence of injection pressure in reacting Spray A, Combust. Flame 191 (2018) 142–159.

[30] B. Tekgül, H. Kahila, O. Kaario, V. Vuorinen, Large-eddy simulation of dual-fuel spray ignition at different ambient temperatures, Combust. Flame 215 (2020) 51–65.

[31] M. Gadalla, J. Kannan, B. Tekgül, S. Karimkashi, O. Kaario, V. Vuorinen, Large-eddy simulation of ECN Spray A: Sensitivity study on modeling assumptions, Energies 13 (13) (2020).

[32] T. Sun, W. Zhao, T. Wang, S. Liao, H. Wei, L. Zhou, Large-eddy simulation of methanol spray combustion characteristics in lean n-heptane mixture environments, Fuel 405 (2026) 136650.

[33] S. Karimkashi, M. Gadalla, J. Kannan, B. Tekgül, O. Kaario, V. Vuorinen, Large-eddy simulation of diesel pilot spray ignition in lean methane-air and methanol-air mixtures at different ambient temperatures, Int. J. Engine Res. 24 (3) (2023) 965–981.

[34] D.G. Goodwin, H.K. Moffat, I. Schoegl, R.L. Speth, B.W. Weber, Cantera: An object-oriented software toolkit for chemical kinetics, thermodynamics, and transport processes, 2024, http://dx.doi.org/10.5281/zenodo.14455267, Version 3.1.0, https://www.cantera.org.

[35] M. Gadalla, J. Kannan, B. Tekgül, S. Karimkashi, O. Kaario, V. Vuorinen, Large-eddy simulation of tri-fuel combustion: Diesel spray assisted ignition of methanol-hydrogen blends, Int. J. Hydrog. Energy 46 (41) (2021) 21687–21703.

[36] J. Kannan, M. Gadalla, B. Tekgül, S. Karimkashi, O. Kaario, V. Vuorinen, Large eddy simulation of diesel spray–assisted dual-fuel ignition: A comparative study on two n-dodecane mechanisms at different ambient temperatures, Int. J. Engine Res. 22 (8) (2021) 2521–2532.

[37] E. Mastorakos, Ignition of turbulent non-premixed flames, Prog. Energy Combust. Sci. 35 (1) (2009) 57–97.

[38] S. Patankar, D. Spalding, A calculation procedure for heat, mass and momentum transfer in three-dimensional parabolic flows, Int. J. Heat Mass Transfer 15 (10) (1972) 1787–1806.

[39] R. Issa, B. Ahmadi-Befrui, K. Beshay, A. Gosman, Solution of the implicitly discretised reacting flow equations by operator-splitting, J. Comput. Phys. 93 (2) (1991) 388–410.

[40] H. Jasak, H. Weller, A. Gosman, High resolution NVD differencing scheme for arbitrarily unstructured meshes, Internat. J. Numer. Methods Fluids 31 (2) (1999) 431–449.

[41] H. Kahila, A. Wehrfritz, O. Kaario, V. Vuorinen, Large-eddy simulation of dual-fuel ignition: Diesel spray injection into a lean methane-air mixture, Combust. Flame 199 (2019) 131–151.

[42] H. Kahila, O. Kaario, Z. Ahmad, M. Ghaderi Masouleh, B. Tekgül, M. Larmi, V. Vuorinen, A large-eddy simulation study on the influence of diesel pilot spray quantity on methane-air flame initiation, Combust. Flame 206 (2019) 506–521.

[43] M. Meijer, L. Somers, J. Johnson, J. Naber, S. Lee, L. Malbec, G. Bruneaux, L. Pickett, M. Bardi, R. Payri, T. Bazyn, Engine combustion network (ECN) : characterization and comparison of boundary conditions for different combustion vessels, Atomization Sprays 22 (9) (2012) 777–806.

[44] L.M. Pickett, J. Manin, C.L. Genzale, D.L. Siebers, M.P.B. Musculus, C.A. Idicheria, Relationship between diesel fuel spray vapor penetration/dispersion and local fuel mixture fraction, SAE Int. J. Engines 4 (1) (2011) 764–799, (Accessed 2025-08-12).

[45] J.V. Pastor, J.M. Garcia-Oliver, A. Garcia, A. Morales López, An experimental investigation on spray mixing and combustion characteristics for spray C/D nozzles in a constant pressure vessel, in: International Powertrains, Fuels and Lubricants Meeting, SAE International, 2018.

[46] H.S. Sim, L. Weiss, N. Maes, L.M. Pickett, High spatiotemporal resolution optical measurements of two-stage ignition and combustion in engine combustion network Spray D flames, Case Stud. Therm. Eng. 62 (2024) 105192.

[47] K. Wan, J. Yi, L. Pickett, J. Manin, Mixing and combustion of methanol and ethanol high-pressure sprays, Exp. Therm. Fluid Sci. 174 (2026) 111704.
[48] N. Maes, S.A. Skeen, M. Bardi, R.P. Fitzgerald, L.-M. Malbec, G. Bruneaux, L.M. Pickett, K. Yasutomi, G. Martin, Spray penetration, combustion, and soot formation characteristics of the ECN Spray C and Spray D injectors in multiple combustion facilities, Appl. Therm. Eng. 172 (2020) 115–136.
[49] G. Karypis, K. Schloegel, V. Kumar, Parmetis: Parallel graph partitioning and sparse matrix ordering library, 1997.
[50] A. Wehrfritz, O. Kaario, V. Vuorinen, B. Somers, Large eddy simulation of n-dodecane spray flames using flamelet generated manifolds, Combust. Flame 167 (2016) 113–131.
[51] R. Payri, J. Gimeno, J. Cuisano, J. Arco, Hydraulic characterization of diesel engine single-hole injectors, Fuel 180 (2016).
[52] O.T. Kaario, V. Vuorinen, H. Kahila, H.G. Im, M. Larmi, The effect of fuel on high velocity evaporating fuel sprays: Large-eddy simulation of Spray A with various fuels, Int. J. Engine Res. 21 (1) (2020) 26–42.
[53] O.T. Kaario, V. Vuorinen, L. Zhu, M. Larmi, R. Liu, Mixing and evaporation analysis of a high-pressure SCR system using a hybrid LES-RANS approach, Energy 120 (2017) 827–841.
[54] A. Wehrfritz, V. Vuorinen, O. Kaario, M. Larmi, Large eddy simulation of high-velocity fuel sprays: Studying mesh resolution and breakup model effects for spray A, At. Sprays 23 (5) (2013) 419–442.
[55] W. Ranz, W. Marshall, Evaporation from Drops-I and II, Chem. Eng. Progr. 48 (1952) 141–146,173–180.
[56] B. Zuo, A.M. Gomes, C.J. Rutland, Studies of superheated fuel spray structures and vaporization in GDI engines, Int. J. Engine Res. 1 (4) (2001) 321–336.
[57] I. Morev, B. Tekgül, M. Gadalla, A. Shahanaghi, J. Kannan, S. Karimkashi, O. Kaario, V. Vuorinen, Fast reactive flow simulations using analytical Jacobian and dynamic load balancing in OpenFOAM, Phys. Fluids 34 (2) (2022) 021801.
[58] B. Tekgül, P. Peltonen, H. Kahila, O. Kaario, V. Vuorinen, DLBFoam: An open-source dynamic load balancing model for fast reacting flow simulations in OpenFOAM, Comput. Phys. Comm. 267 (2021) 108073.
[59] A. Haider, I. Morev, A. Rintanen, Z. Shahin, P. Tamadonfar, S. Karimkashi, A. Wehrfritz, V. Vuorinen, Accelerated numerical simulations of hydrogen flames: Open-source implementation of an advanced diffusion model library in OpenFOAM, Int. J. Hydrog. Energy 189 (2025) 152115.
[60] A. Frassoldati, G. D'Errico, T. Lucchini, A. Stagni, A. Cuoci, T. Faravelli, A. Onorati, E. Ranzi, Reduced kinetic mechanisms of diesel fuel surrogate for engine CFD simulations, Combust. Flame 162 (10) (2015) 3991–4007.
[61] Y. Zeldovich, D. Frank-Kamenetskii, P. Sadovnikov, Oxidation of Nitrogen in Combustion, Publishing House of the Acad of Sciences of USSR, 1947.
[62] G.A. Lavoie, Spectroscopic measurements of nitric oxide in spark ignition engines, Combust. Flame 15 (2) (1970) 97–108.
[63] M. Abian, M.U. Alzueta, P. Glarborg, Formation of NO from N_2/O_2 mixtures in a flow reactor: Toward an accurate prediction of thermal NO, Int. J. Chem. Kinet. 47 (8) (2015) 518–532.
[64] Ø. Skreiberg, P. Kilpinen, P. Glarborg, Ammonia chemistry below 1400K under fuel-rich conditions in a flow reactor, Combust. Flame 136 (4) (2004) 501–518.
[65] A. Fernandez, A. Goumri, A. Fontijn, Kinetics of the reactions of N(4S) atoms with O_2 and CO_2 over wide temperatures ranges, J. Phys. Chem. A 102 (1) (1998) 168–172.
[66] R. Eliseo, F. Alessio, S. Alessandro, P. Matteo, C. Alberto, F. Tiziano, Reduced kinetic schemes of complex reaction systems: Fossil and biomass-derived transportation fuels, Int. J. Chem. Kinet. 46 (9) (2014) 512–542.
[67] E. Ranzi, C. Cavallotti, A. Cuoci, A. Frassoldati, M. Pelucchi, T. Faravelli, New reaction classes in the kinetic modeling of low temperature oxidation of n-alkanes, Combust. Flame 162 (5) (2015) 1679–1691.
[68] G. Bagheri, E. Ranzi, M. Pelucchi, A. Parente, A. Frassoldati, T. Faravelli, Comprehensive kinetic study of combustion technologies for low environmental impact: MILD and OXY-fuel combustion of methane, Combust. Flame 212 (2020) 142–155.
[69] A. Frassoldati, T. Faravelli, E. Ranzi, Kinetic modeling of the interactions between NO and hydrocarbons at high temperature, Combust. Flame 135 (1) (2003) 97–112.
[70] T. Faravelli, A. Frassoldati, E. Ranzi, Kinetic modeling of the interactions between NO and hydrocarbons in the oxidation of hydrocarbons at low temperatures, Combust. Flame 132 (1) (2003) 188–207.
[71] L.M. Pickett, C.L. Genzale, J. Manin, Uncertainty quantification for liquid penetration of evaporating sprays at diesel-like conditions, At. Sprays 25 (5) (2015) 425–452.
[72] J. Shao, R. Choudhary, Y. Peng, D.F. Davidson, R.K. Hanson, A shock tube study of n-heptane, iso-octane, n-dodecane and iso-octane/n-dodecane blends oxidation at elevated pressures and intermediate temperatures, Fuel 243 (2019) 541–553.
[73] L. Cai, Y. Uygun, C. Togbé, H. Pitsch, H. Olivier, P. Dagaut, S.M. Sarathy, An experimental and modeling study of n-octanol combustion, Proc. Combust. Inst. 35 (1) (2015) 419–427.
[74] S. Karimkashi, H. Kahila, O. Kaario, M. Larmi, V. Vuorinen, Numerical study on tri-fuel combustion: Ignition properties of hydrogen-enriched methane-diesel and methanol-diesel mixtures, Int. J. Hydrog. Energy 45 (7) (2020) 4946–4962.
[75] M. Gadalla, S. Karimkashi, I. Kabil, O. Kaario, T. Lu, V. Vuorinen, Embedded direct numerical simulation of ignition kernel evolution and flame initiation in dual-fuel spray assisted combustion, Combust. Flame 259 (2024) 113172.
[76] S. Karimkashi, H. Kahila, O. Kaario, M. Larmi, V. Vuorinen, A numerical study on combustion mode characterization for locally stratified dual-fuel mixtures, Combust. Flame 214 (2020) 121–135.
[77] R. Bilger, Turbulent jet diffusion flames, Prog. Energy Combust. Sci. 1 (2) (1976) 87–109.
[78] Y. Mao, M. Raza, Z. Wu, J. Zhu, L. Yu, S. Wang, L. Zhu, X. Lu, An experimental study of n-dodecane and the development of an improved kinetic model, Combust. Flame 212 (2020) 388–402.
[79] Y. Pei, S. Som, E. Pomraning, P.K. Senecal, S.A. Skeen, J. Manin, L.M. Pickett, Large eddy simulation of a reacting spray flame with multiple realizations under compression ignition engine conditions, Combust. Flame 162 (12) (2015) 4442–4455.
[80] C.K. Westbrook, W.J. Pitz, O. Herbinet, H.J. Curran, E.J. Silke, A comprehensive detailed chemical kinetic reaction mechanism for combustion of n-alkane hydrocarbons from n-octane to n-hexadecane, Combust. Flame 156 (1) (2009) 181–199.
[81] S.M. Sarathy, P. Oßwald, N. Hansen, K. Kohse-Höinghaus, Alcohol combustion chemistry, Prog. Energy Combust. Sci. 44 (2014) 40–102.